THE ASTROPHYSICAL JOURNAL, 456:631–643, 1996 January 10

INFRARED EMISSIVITY OF HD IN MAGNETOHYDRODYNAMIC SHOCKS

RALF TIMMERMANN[1]
University of Arizona, Lunar and Planetary Laboratory, Tucson, AZ 85721
Received 1993 January 15; accepted 1995 July 17

ABSTRACT

A discussion of IR line emission of deuterated hydrogen HD that emanates from regions of shocked molecular gas (C type) is presented. Results are given for shock speeds of $15 < u_s < 45$ km s^{-1} and preshock densities of $10^4 < n_H < 10^6$ cm^{-3}, where all available data for HD to date are utilized. We find that a fraction of HD is converted to atomic deuterium in the hot postshocked gas with $u_s \gtrsim 30$ km s^{-1} when H_2 becomes sufficiently dissociated. However, a part of this atomic deuterium is recovered to HD through chemical reactions with H_2 when the shocked gas cools down again. Measurements of HD line intensities may be used to derive its abundance in the dense interstellar medium (ISM). Having assumed a deuterium abundance of $HD/H_2 = 3.0 \times 10^{-5}$ for the ISM we find that line emission of HD may be detectable with currently available IR spectrometers at ground-based telescopes when the preshock densities are $n_H \gtrsim 10^5$ cm^{-3}. *ISO* may even observe rotational transitions of HD from less dense gas.

Subject headings: ISM: abundances — ISM: jets and outflows — ISM: molecules — shock waves

1. INTRODUCTION

Owing to the tremendous improvement in sensitivity, IR spectrometers may now observe, besides line emission of molecular hydrogen, also line emission of its deuterated counterpart HD in the interstellar medium (ISM). Observations of HD in the ISM would be of great interest, in particular for cosmological reasons, since probably a huge fraction of the primordial deuterium is locked in this molecular form. A deduction of the D/H ratio through the measurement of HD emission lines would result in a lower limit to its primordial ratio, according to the standard theory that deuterium was only produced during big bang nucleosynthesis and is steadily destroyed in stars thereafter. The abundance of deuterium in the ISM is believed to be $5 \times 10^{-6} < D/H < 2 \times 10^{-5}$ (York & Rogerson 1976; Vidal-Madjar et al. 1977, 1982, 1983; Laurent, Vidal-Madjar, & York 1979). In a recent reevaluation of previously published Lyman absorption-line measurements McCullough (1992) found a value of $D/H = (1.5 \pm 0.2) \times 10^{-5}$. It also appeared that this ratio is constant in the local ISM. New results with the *Hubble Space Telescope* established $D/H = (1.65^{+0.07}_{-0.18}) \times 10^{-5}$ for the ISM toward double star Capella (Linsky et al. 1993). This value was confirmed later (Linsky et al. 1994), whereas $D/H = (1.40 \pm 0.10) \times 10^{-5}$ for Procyon was found.

HD reveals, unlike its homonuclear counterpart H_2, a weak dipole moment that is due to nonadiabatic effects, coupling electronic and nuclear motions. This leads to radiative transitions that are, by rule of thumb, about 2 orders of magnitude faster then quadrupole transitions (of similar transition energies) of H_2. Just by comparing the radiative transition probabilities of H_2 and HD it seems that this effect can only partially offset the low abundance of HD. Its line emission strength still appears to remain smaller by roughly 3 orders of magnitude. Nevertheless, Shull & Beckwith (1982) suggested that line emission of HD may be observed, however, in objects that show very strong H_2 emission. Line emission of H_2 is observed either from photon-heated surfaces of dense clouds or from gas with temperatures greater than ~ 500 K that was heated through the passage of a shock front. In the former case hydrogen molecules are excited electronically via absorption of UV photons into their Lyman and Werner bands that is followed by rapid radiative decay into bound rovibrational states of the electronic ground state, producing fluorescent line emission. In the case of shock heating these rovibrational states are populated via collisions in the hot gas, which subsequently decay radiatively.

It was recently shown (Sternberg 1990) that fluorescent line emission of HD can emanate from dense photodominated regions that arise from strong UV illumination. It was demonstrated that only from sufficiently dense regions ($n_H \gtrsim 5 \times 10^6$ cm^{-3}) such as the Orion bright bar the intensity of HD line emission in the *H* band (1.45–1.80 μm) is strong enough to be detectable. We point out, however, that with the exception of UV observations in diffuse clouds (Wright & Morton 1979), HD has not yet been detected via its IR line emission to date. In order to seek evidence of interstellar HD through IR radiation shocked dense molecular gas would offer a good possibility. Since to our knowledge this scenario has not yet received adequate attention in the literature we want to explore it in the present paper. In the following we consider only C type magnetohydrodynamic (MHD) shocks in dense molecular gas. The shock velocities are chosen such that molecular hydrogen is not yet completely dissociated. MHD shocks were discussed in detail by Draine (1980), Draine, Roberge, & Dalgarno (1983), Flower, Pineau des Forets, & Hartquist (1985, 1986), and Smith & Brand (1990a, b). In our attempt to calculate the strengths of IR line emission of HD we will follow the basic ideas of Flower et al. (1985, 1986) in the treatment of the shock parameters. Their model is extended such that also HD is included by utilizing all data available to date. Furthermore, it will be examined whether selected radiative transitions in the $v = 1 \rightarrow 0$ and $0 \rightarrow 0$ bands can indeed be detected with state-of-the-art near- or mid-IR spectrometers from ground-based telescopes or with the *Infrared Space Observatory* (*ISO*).

[1] Postal address: Max-Planck-Institut für Extraterrestrische Physik, 85740 Garching, Germany; timmer@mpe-garching.mpg.de.

2. SHOCK MODEL

2.1. *Basic Equations*

We considered a steady plane-parallel shock wave, with shock speed u_s, running into dense uniform molecular gas of preshock density $n_H = n(H) + 2n(H_2)$. The flow velocities of the neutral and ionized gas, u_n and u_i, are expressed in the frame of reference in which the shock wave is stationary. A three-fluid model for the shocked medium was considered. In the following we define the basic conservation equations for the shock wave. We start with the conservation of particle number density for neutrals and ions:

$$\frac{d}{dz}\left(\frac{\rho_n u_n}{\mu_n}\right) = N_n\,, \tag{1}$$

$$\frac{d}{dz}\left(\frac{\rho_i u_i}{\mu_i}\right) = N_i\,, \tag{2}$$

where ρ_n, ρ_i are the total mass densities and μ_n, μ_i the mean weights for neutrals and ions, respectively. The variable z denotes the independent variable along the flow direction that is parallel to the line of sight of the observer. The conservation equation for the electrons is identical to equation (2). The following equations,

$$\frac{d}{dz}(\rho_n u_n) = S_n \tag{3}$$

and

$$\frac{d}{dz}(\rho_i u_i) = S_i\,, \tag{4}$$

describe the conservation of mass and

$$\frac{d}{dz}\left(\rho_n u_n^2 + \frac{\rho_n k T_n}{\mu_n}\right) = A_n\,, \tag{5}$$

$$\frac{d}{dz}\left[\rho_i u_i^2 + \frac{\rho_i k(T_i + T_e)}{\mu_i} + \frac{B_0^2}{8\pi}\left(\frac{u_s}{u_i}\right)^2\right] = A_i\,, \tag{6}$$

denote the conservation of momentum for neutrals and ions, respectively. T_n, T_i, and T_e are the kinetic temperatures for the neutrals, ions, and electrons and k is the Boltzmann constant. The interstellar magnetic field B_0 was assumed to be perpendicular to the incoming shockwave and frozen into the ionized gas. Thus, we can calculate the magnetic field in the shocked region downstream via $B = B_0(u_s/u_i)$. This is already included in equations (6), (8), and (9). The energy conservation equations for neutrals, ions, and electrons are

$$\frac{d}{dz}\left(\frac{1}{2}\rho_n u_n^3 + \frac{5}{2}\frac{\rho_n u_n k T_n}{\mu_n} + \frac{\rho_n u_n U_n}{\mu_n}\right) = B_n\,, \tag{7}$$

$$\frac{d}{dz}\left(\frac{1}{2}\rho_i u_i^3 + \frac{5}{2}\frac{\rho_i u_i k T_i}{\mu_i} + \frac{B_0^2}{4\pi}\frac{u_s^2}{u_i}\right) = B_i\,, \tag{8}$$

$$\frac{d}{dz}\left[\frac{1}{2}\rho_i u_i^3 + \frac{5}{2}\frac{\rho_i u_i k(T_i + T_e)}{\mu_i} + \frac{B_0^2}{4\pi}\frac{u_s^2}{u_i}\right] = B_i + B_e\,. \tag{9}$$

U_n describes the internal energy of the neutral gas, which is in our case due to the population of excited states in H_2 (see § 3). The significance of the source terms N, S, A, and B will be discussed in the next section. One equation, describing the conservation of the individual species such as molecules, atoms, and ions has to be added by utilizing

$$\frac{d}{dz}(n_\alpha u_\alpha) = C_\alpha\,, \tag{10}$$

where

$$C_\alpha = \sum_\beta C_{\alpha\beta} \tag{11}$$

and n_α denotes the number density of species α and C_α its formation rate that is described as the sum over all chemical reactions β in which α participates.

2.2. *Source Terms*

The significance of the source terms has already been discussed in full detail (Flower et al. 1985, 1986). We will, therefore, only summarize their definition of the source terms. N_n and N_i are the number of particles transferred from the ionized to neutral fluid and from the neutral to the ionized fluid, respectively, where

$$N_n = \sum_\alpha^{\text{neutrals}} C_\alpha \tag{12}$$

and

$$N_i = \sum_\alpha^{\text{ions}} C_\alpha \tag{13}$$

Similarly, S_n and S_i are the rates for the mass transferred from the ionized to the neutral fluid and vice versa, respectively, where

$$S_n = \sum_\alpha^{\text{neutrals}} C_\alpha m_\alpha\,, \tag{14}$$

$$S_i = \sum_\alpha^{\text{ions}} C_\alpha m_\alpha\,, \tag{15}$$

with $S_i = -S_n$ and m_α is the mass of species α. We define the rate A_n as the momentum transferred to the neutrals with $A_n = A_{n1} + A_{n2}$ and $A_i = -A_n$. A_{n1} denotes the rate due to reactive collisions

$$A_{n1} = \sum_\alpha^{\text{neutrals}} \sum_\beta C_{\alpha\beta} m_\alpha u_\beta\,, \tag{16}$$

where u_β is the center-of-mass velocity with $u_\beta = u_n$, $u_\beta = u_i$, or $u_\beta = (m_i u_i + m_n u_n)/(m_i + m_n)$ if the reactants are both neutrals, both ions, or neutral and ion, respectively. The momentum transfer to the neutral fluid due to elastic scattering between ions and neutrals (Osterbrock 1961) is

$$A_{n2} = \frac{\rho_i \rho_n}{\mu_i + \mu_n}\langle\sigma v\rangle_{in}(u_i - u_n)\,, \tag{17}$$

where the collision rate coefficient for $v < 24$ km s^{-1} is

$$\langle\sigma v\rangle_{in} = 2.41\pi e\left(\frac{\alpha_n}{\mu_{in}}\right)^{1/2}\,, \tag{18}$$

with $\mu_{in} = m_i m_n/(m_i + m_n)$ describing the reduced mass and e is the charge of the electron. The polarizability of H, He, and H_2 is $\alpha_n = 6.67 \times 10^{-25}$, 2.07×10^{-25}, and 8.04×10^{-25} cm^3, respectively. For higher velocities $v > 24$ km s^{-1} (Draine 1980) the rate coefficient becomes

$$\langle\sigma v\rangle_{in} \approx 10^{-15}\ \text{cm}^2\ v\,, \tag{19}$$

where

$$v = \left[\frac{8k}{\pi}\left(\frac{T_n}{m_n} + \frac{T_i}{m_i}\right) + (u_i - u_n)^2\right]^{1/2}. \quad (20)$$

Now we consider all source terms that involve the energy transfer between the fluids. We define $B_n = \sum_j B_{nj}$, $B_i = \sum_j B_{ij}$, and $B_e = \sum_j B_{ej}$. Kinetic energy due to chemical reactions is transferred to the neutrals and ions at rates

$$B_{n1} = \sum_{\alpha}^{\text{neutrals}} \sum_{\beta} \tfrac{1}{2} C_{\alpha\beta} m_\alpha u_\beta^2 \quad (21)$$

and

$$B_{i1} = \sum_{\alpha}^{\text{ions}} \sum_{\beta} \tfrac{1}{2} C_{\alpha\beta} m_\alpha u_\beta^2 . \quad (22)$$

Moreover, we have included the transfer of enthalpy between the fluids, where

$$B_{n2} = \sum_{\alpha}^{\text{neutrals}} \left[\sum_{\beta} \tfrac{5}{4} k(T_i + T_e) C_{\alpha\beta}(C_{\alpha\beta} > 0) + \sum_{\beta} \tfrac{5}{2} k T_n C_{\alpha\beta}(C_{\alpha\beta} < 0)\right] \quad (23)$$

is the rate at which energy is transferred to the neutrals,

$$B_{i2} = \sum_{\alpha}^{\text{ions}} \left[\sum_{\beta} \tfrac{5}{2} k T_n C_{\alpha\beta}(C_{\alpha\beta} > 0) + \sum_{\beta} \tfrac{5}{2} k T_i C_{\alpha\beta}(C_{\alpha\beta} < 0)\right] \quad (24)$$

is the rate for the ions, and

$$B_{e2} = \sum_{\alpha}^{\text{ions}} \sum_{\beta} \tfrac{5}{2} k T_e C_{\alpha\beta} \quad (C_{\alpha\beta} < 0) \quad (25)$$

is the energy transfer rate to the electrons. We note that neither these rates nor the previous ones (B_{n1} and B_{i1}) play an important role at densities considered in the present model. This also applies for the momentum transfer (A_{n1}). However, these rates will become more important at lower densities. Energy is also deposited in the gas by cosmic-ray ionization. We, therefore, apply the rates for the heating of the neutral and electron fluid (Draine et al. 1983)

$$B_{n3} = 8.46 \times 10^{-12} \zeta [n(\mathrm{H}) + 2n(\mathrm{H_2})] \text{ ergs s}^{-1} \text{ cm}^{-3}, \quad (26)$$

$$B_{e3} = 4.23 \times 10^{-12} \zeta [n(\mathrm{H}) + 2n(\mathrm{H_2})], \quad (27)$$

where ζ is the cosmic-ray primary ionization rate. For the purpose of this paper we used $\zeta = 5 \times 10^{-17}$ s^{-1}. Energy is mainly transferred through elastic scattering between ions and neutrals, where

$$B_{n4} = \frac{\rho_n \rho_i}{(\mu_i + \mu_n)^2} \langle \sigma v \rangle_{in} \times \left[\frac{3}{2} k(T_i - T_n) + \frac{1}{2}(u_i - u_n)(\mu_i u_i + \mu_n u_n)\right] \quad (28)$$

and $B_{i4} = -B_{n4}$. For the energy transfer between the neutral and electron fluids we utilized the rate

$$B_{n5} = \frac{\rho_n \rho_i}{\mu_i \mu_n} \langle \sigma v \rangle_{en} \frac{2m_e}{\mu_n} \left[2k(T_e - T_n) + \frac{1}{2} \mu_n u_n (u_i - u_n)\right], \quad (29)$$

where

$$\langle \sigma v \rangle_{en} = 10^{-15} \text{ cm}^2 \left(\frac{8kT_e}{\pi m_e}\right)^{1/2}, \quad (30)$$

m_e is the mass of the electron, and $B_{e5} = -B_{n5}$. Energy transfer due to scattering amongst the ion and electron fluids is calculated by

$$B_{e6} = \frac{4e^4}{\mu_i T_e} \left(\frac{2\pi m_e}{kT_e}\right)^{1/2} \ln(\Lambda) \left(\frac{\rho_i}{\mu_i}\right)^2 (T_i - T_e), \quad (31)$$

where

$$\Lambda = \frac{3}{2e^3} \left(\frac{k^3 T_e^3 \mu_i}{\pi \rho_i}\right)^{1/2} \quad (32)$$

and analogously $B_{i6} = -B_{e6}$. So far we have not yet considered the cooling of the individual fluids due to radiation. We will describe these processes in § 2.3. Charged dust grains may become important in the coupling of momentum from the magnetic field to the neutrals if the fractional ionization is low (Draine 1980). We have therefore also considered its contribution in our model by applying his equations (40) and (42) for the momentum (A_{n7}) and energy transfer (B_{n7}). For the calculation of the dust temperature we assumed the Planck-averaged absorption efficiency (Draine 1987) for silicates of radius $a = 5 \times 10^{-5}$ cm and a standard interstellar radiation field. The dust density was 3 g cm^{-3} and $\rho_{\text{dust}}/\rho_{\text{gas}} = 6 \times 10^{-3}$. The current model neglected that a part of the energy released in the formation of H_2 may heat the dust grains.

2.3. *Cooling Processes*

When the neutral gas component of the dense molecular cloud is heated through collisions, excited levels in molecules and atoms are populated. Subsequently, these levels decay via radiative transitions, leading to the cooling of the gas. For high shock velocities, energy losses occur mainly through cooling due to H_2O, H_2, and CO. At low shock speeds mainly fine-structure lines contribute to the cooling. Radiative cooling through H_2 becomes important only when its rotational and vibrational levels are sufficiently populated. The rate at which the neutral gas cools due to radiative transitions in H_2 is expressed through

$$B_{\text{rad}}(\mathrm{H_2}) = -\sum_{v,J} n_{v,J} A_{v,J \to v',J'} \Delta E, \quad (33)$$

where $\Delta E = E_{v,J} - E_{v',J'}$ is the level energy difference. The population probability of levels $n_{v,J}$ in H_2 is discussed in § 3. Contributions to the cooling by line emission of HD has been neglected. When H_2 is dissociated (see § 4), the neutral gas is cooled since an energy of $E_{\text{diss}} = 4.48$ eV per molecule is needed to overcome its molecular binding. The cooling function due to dissociation of H_2 can be described via

$$B_{\text{diss}}(\mathrm{H_2}) = -7.18 \times 10^{-12} n(\mathrm{H_2}) D \text{ ergs s}^{-1} \text{ cm}^{-3}, \quad (34)$$

where D is the dissociation rate of H_2 in s^{-1}. For radiative losses of the neutral fluid due to H_2O we applied the formalism of Neufeld & Melnick (1987) for their large velocity gradient case where $\eta = \max [du_n/dz, 10^{-13} \text{ s}^{-1}]$. The latter number represents the value for the microturbulence in molecular clouds of 3 km s^{-1} pc^{-1}. The equations for radiative cooling through rotational transitions in CO are adopted from McKee et al. (1982) and Hollenbach & McKee (1979), and for vibrational transitions in CO from Hollenbach & McKee (1989). Furthermore, we have included the radiation losses due to OH based on the calculation by Hollenbach & McKee (1979). In order to compute the cooling also for low shock speeds we have adopted its cooling rates for the neutral gas for fine-

structure lines of C, C^+, and O as described in Flower et al. (1986). We also utilized their rates for the cooling of the electron fluid.

3. LEVEL POPULATION PROBABILITIES IN HD AND H_2

In order to calculate the intensity of H_2 and HD line emission we had to know the population of all rovibrational states in these molecules. Therefore, we first created a three level system in which we collapsed all rotational levels into one state for the vibrational levels $v = 0$, 1, and 2. The population probabilities of vibrational levels of HD and H_2 were obtained by calculating statistical equilibrium maintained by collisional excitations, deexcitations and radiative transitions. It has been neglected that selective depopulations or populations of rovibrational levels may occur through collision-induced dissociation and chemical reactions. We defined the following level parameters for H_2 and HD: $g_0 = g_1 = g_2 = 1$. For the vibrational levels in H_2 we adopted $E_{10}/k = 6000$ and $E_{20}/k =$ 11,630 K with radiative lifetimes $A_{10} = 8.3 \times 10^{-7}$, $A_{20} = 4.1 \times 10^{-7}$, and $A_{21} = 1.1 \times 10^{-6}$ s^{-1}. The level parameters of HD are $E_{10}/k = 5230$ and $E_{20}/k = 10{,}200$ K with radiative lifetimes $A_{10} = 4.1 \times 10^{-5}$, $A_{20} = 4.1 \times 10^{-6}$, and $A_{21} = 6.3 \times 10^{-5}$ s^{-1}. The energies of all vibrational and rotational states in HD and H_2 have been taken from McKellar, Goetz, & Ramsey (1976), Margolis (1980) and Bragg, Brault, & Smith (1982). For the lifetimes of radiative transitions in HD and H_2 we employed the values of Abgrall, Roueff, & Viala (1982) and Turner, Kirby-Docken, & Dalgarno (1977), respectively. The values A_{ij}, used above, were obtained by averaging the radiative lifetimes of all rotational states for each vibrational level. The rate coefficients for vibrational deexcitations of H_2, which include He–H_2, H_2–H_2, and H–H_2 collisions, have been adopted from Table 2 of Draine et al. (1983). The rate coefficients for collisional excitation were calculated by applying the principles of detailed balance theory. For the evaluation of collisional deexcitation rates from vibrational levels of HD we employed the result obtained in a shock tube experiment (Simpson, Price, & Crowther 1975). The vibrational relaxation times of HD in hot gas with temperatures of 1950 and 1630 K were found to be 2 times faster than that of H_2 or D_2. The results of this measurement and a theoretical work on relaxation times in He–HD (Tarr & Rabitz 1979) would seem to indicate that contributions by rotational motion is more effective for vibrational-rotational-translational energy exchange owing to a larger number of rovibrational pathways in HD. In fact, the large distribution of final rotational states is a result of the smaller rotational constant of HD and a more anisotropic potential occurring in M–HD compared to that of M–H_2. Unfortunately, it appears that the result of Tarr & Rabitz, only when compared to calculated relaxation times in He–H_2 (Rabitz & Zarur 1975), does not agree with the experimental findings. In fact, the rate coefficient in He–HD turned out to be 5 times lower than that of He–H_2 at a temperature of 500 K. However, Tarr and Rabitz pointed out that the relaxation times of both systems cannot be directly compared since both calculations indicate an increased sensitivity of the relaxation times at such low temperatures due to different potentials and computational methods applied to both systems. Considering the apparent uncertainties in these calculations we thus disregarded the theoretical rate coefficients and relied on the experimental results instead. For the evaluation of all M–HD deexcitational rate coefficients we therefore introduced a factor $\alpha = 2$ by which all rates of He–HD, H_2–HD, and H–HD are greater than that of He–H_2, H_2–H_2, and H–H_2, respectively. In § 5.3 we will examine the impact of the M–HD rate coefficients on the line intensities of HD.

Once the population distribution of the vibrational levels in HD and H_2 were established we determined that of the rotational states J, whereby 14 states for each vibrational level were included in our calculations. For the rotational deexcitation ($\Delta J = -2$) in H_2 via collision with H and H_2

$$\langle \sigma v \rangle_{J \to J-2} = 4.6 \times 10^{-12}(2J - 3)T_n^{1/2}(1 + x)^{1/2} \times \exp\left[\frac{-5.01x}{1 + E_J/kT_n} - 0.1187(4J - 2)\right] \text{cm}^3 \text{ s}^{-1} \quad (35)$$

was adopted (Elitzur & Watson 1978; Flower et al. 1986), where

$$x = \Delta E/kT_n \quad (36)$$

and $\Delta E = E_J - E_{J-2}$. Thus, we get

$$r_{J \to J-2} = n_J[n(\text{H}) + n(\text{H}_2) + 0.87n(\text{He})]\langle \sigma v \rangle_{J \to J-2} \text{ cm}^{-3} \text{ s}^{-1} \quad (37)$$

for the rate coefficient. The rate coefficients for He we adopted are an educated guess from the ratios of the reduced masses. In this regard, however, we should point out the calculations by Danby, Flower, & Monteiro (1987) who find that the He–H_2 rate coefficient is similar to the value for ortho-H_2($J = 1$)–H_2 at $T_n = 100$ K, whereas it is even larger by typically a factor of about 1.5 at $T_n = 500$ K. Considering only radiative and collisional transitions between the rotational levels we can write for the equilibrium

$$\frac{d}{dt} n_J = (r_{J+2 \to J} + A_{J+2 \to J})n_{J+2} + r_{J-2 \to J} n_{J-2} - (r_{J \to J+2} + r_{J \to J-2} + A_{J \to J-2})n_J \,. \quad (38)$$

The ortho-para ratio in H_2 was fixed to 3 and ortho- and para-H_2 were treated as two separate systems. The internal energy U_n in equation (7) that is due to excited levels in H_2 can now be determined to

$$\frac{\rho_n}{\mu_n} U_n = \sum_{v,J} n_{v,J} E_{v,J} \,. \quad (39)$$

For the evaluation of the rate coefficients of HD we employed the cross sections of He–HD and H_2–HD provided by Schaefer (1990). Since these data cover only rotational states $J < 5$ we extrapolated these rate coefficients also to higher rotational levels. As it has been indicated by Schaefer the cross sections for deexcitation from higher rotational states $J > 4$ can be simply derived from that of lower states by applying the proper detailed balance formula. For our calculations we considered only cross sections for deexcitations with $\Delta J = -1$ and -2 since those for $\Delta J = -3$ are already smaller by about 1 order of magnitude. We fitted the rate coefficients for collisional deexcitation in He–HD to

$$\langle \sigma v \rangle = 7.2 \times 10^{-4} T_n^{-1.5} \frac{2J - 1}{2J + 1} \int_0^\infty E \exp - \left[\frac{(4.99 \times 10^{-2} + 1.71\Delta E)^2}{E} + \frac{E}{kT_n}\right] dE \quad (40)$$

for $J \rightarrow J - 1$, and

$$\langle \sigma v \rangle = 3.7 \times 10^{-4} T_n^{-1.5} \frac{2J-3}{2J+1} \int_0^\infty E \exp - \left[\frac{(9.80 \times 10^{-2} + 1.98\Delta E)}{E} + \frac{E}{kT_n} \right] dE \quad (41)$$

for $J \rightarrow J - 2$, where ΔE denotes the energy difference between the upper and lower states in units of eV. We expect the fits of equations (40) and (41) to be accurate within 50% for temperatures $250 < T_n < 10^4$ K and $J < 6$, whereas they become less accurate for higher levels at low temperatures. Uncertainties in the rate coefficients for higher quantum states $J > 6$ arise because it is not well known at which energy the cross sections, which are roughly constant at high energies, actually decrease at lower energies (see Fig. 4 of Schaefer). However, since the population probabilities of high rotational states $J > 6$ become small at low temperatures, uncertainties in the rates are expected not to affect the results of our calculations. Schaefer also noticed that the H_2–HD rate coefficient can be derived from the He–HD rates as well. It turns out that the cross section (vs. energy) of H_2– HD collisional deexcitation is similar to that of He–HD. Hence, the rate coefficient of H_2–HD be can simply calculated by $\langle \sigma v \rangle_{H_2-HD} = (\mu_{He-HD}/\mu_{H2-HD})^{1/2} \langle \sigma v \rangle_{He-HD}$, where μ denotes the reduced mass and $(\mu_{He-HD}/\mu_{H_2-HD})^{1/2} = 1.19$. We notice that the H_2–HD rate, when calculated by this method, deviates by about 10% from the actual rates (see Schaefer) at a temperature of 200 K, whereas this deviation diminishes toward higher temperatures. Since to our knowledge no rate coefficients for the rotational deexcitation of the system H–HD are available in the literature we calculated this rate by the same method as used above, where $\langle \sigma v \rangle_{H-HD} = (\mu_{He-HD}/\mu_{H-HD})^{1/2} \langle \sigma v \rangle_{He-HD}$ with $(\mu_{He-HD}/\mu_{H-HD})^{1/2} = 1.51$. This assumption, however, is an educated guess, and data on H–HD are urgently needed. One might expect that the H–HD collision cross sections are similar to those of H–H_2 (Mandy & Martin 1991). However, according to these authors all transitions $H + H_2(\text{para}) \rightarrow H_2(\text{ortho}) + H$ can only occur via exchange of a hydrogen atom, thus, creating a large dynamic threshold. For instance the barrier energy for $H + H_2(J = 0) \rightarrow H_2(J = 1) + H$ is 0.424 eV, whereas the energy difference between these two levels in H_2 is just 0.015 eV. We therefore hesitated to apply the H–H_2 rates for the purposes of our model since for the reaction $H + HD(J) \rightarrow HD(J + 1) + H$ the situation is quite different.

4. CHEMISTRY IN THE POSTSHOCKED GAS

When a shock wave travels through the dense ISM the composition of the fluids changes due to chemical reactions. A substantial difference in flow velocities of ions and neutrals in certain regions causes some of the ion-neutral reactions, which are usually inhibited due to high-energy thresholds, to become important. For instance, Flower et al. (1985) have investigated the effect on the shock structure when the fractional ionization decreases as a result of

$$C^+ + H_2 \rightarrow CH^+ + H\,, \quad (42)$$

$$CH^+ + e \rightarrow C + H\,, \quad (43)$$

whose net result is a neutralization of C^+. Similarly, as the neutral gas is heated reactions among neutrals can proceed at much higher rates. Draine et al. (1983) have shown that endothermic reactions such as

$$H_2 + O \rightarrow OH + H \quad (44)$$

$$H_2 + OH \rightarrow H_2O + H \quad (45)$$

can convert all available neutral oxygen into H_2O once the neutral gas temperature is $T_n \gtrsim 500$ K. Since the produced H_2O then cools warm gas very efficiently, the shock structure can be modified significantly. For $T_n < 1000$ K, where vibrational levels of H_2 are not yet appreciably excited, the temperature of the neutral postshock gas is mainly controlled by the strength of H_2O line emission. All above reactions have been included into our model calculations (see Table 2 below).

In order to compute the intensity of HD line emission that emanates from shocked molecular gas, we also needed to incorporate its chemistry into our model. Deuterium chemistry in shocks has been described in Pineau des Forets, Roueff, & Flower (1989), where these authors mainly focus on fractionation effects in dark clouds. For the purpose of our model we utilized some of their reactions, in particular those that involve the formation and destruction of HD (see Table 2, below). As ion-neutral reactions are important for gas of lower density, neutral-neutral reactions dominate the chemistry at higher densities and temperatures. It appears that the abundance of HD in shocked dense gas is mainly affected by the chemical exchange reaction

$$HD + H \rightleftharpoons H_2 + D \quad (46)$$

with atomic hydrogen (Dalgarno 1985a,b). H is supplied by dissociation of H_2 in the postshock region through

$$M + H_2 \rightarrow M + H + H\,, \quad (47)$$

where M is a neutral or ionized species. Equation (46) is endothermic and implies that HD can reform again from deuterium if appreciable amounts of H_2 are still present in the cooling neutral gas. We found the rate coefficients for the *reverse reaction* of equation (46) to $r_{H_2+D} = 1.6 \times 10^{-10} \exp(-3876\ \text{K}/T_n)$ and $3.1 \times 10^{-10} \exp(-1611\ \text{K}/T_n)$ cm^3 s^{-1} for H_2 in its ground and first vibrational state, respectively (Rozenshtein et al. 1985). The latter rate was not used in our model calculations since only a small fraction of H_2 is found in its first vibrational state when temperatures of $T_n \lesssim 2500$ K are reached in the postshocked gas. We note that these rates represent also the high-temperature regimes of T_n quite well. A comparison with the rate of Götting, Mayne, & Toennies (1986) reveals that the rate of Rozenshtein et al. is lower by a factor of 2.3 for H_2 ($v = 0$) at $T_n \approx 10^4$ K. For completion, we also quote the rate coefficients for the *reverse direction* of equation (46) provided by other authors. Zhang & Miller (1989) calculate rates that are higher than those used here by a factor of 1.7 and 2.1 for temperatures of 1000 and 500 K, respectively, while Westenberg & de Haas (1967) give a rate of $\langle \sigma v \rangle_{H_2+D} = 7.3 \times 10^{-11} \exp(-3830\ \text{K}/T_n)$. Schofield (1967) and Mitchell & LeRoy (1973) imply rates of $4.3 \times 10^{-11} \exp(-3413\ \text{K}/T_n)$ and $2.7 \times 10^{-17} T_n^2 \exp(-2698\ \text{K}/T_n)$ cm^3 s^{-1}, respectively. Still interesting to note that the value for the cross section of $D + H_2 \rightarrow HD(v = 1) + H$ has been calculated to be about 11% of that for $D + H_2 \rightarrow HD(v = 0) + H$ at temperatures above 10^4 K (Continetti, Balko, & Lee 1990). Shavitt (1959) measure for the rate coefficient of the *forward reaction* equation (46) $\langle \sigma v \rangle_{HD+H} = 3.2 \times 10^{-11} \exp(-3624\ \text{K}/T_n)$ cm^3 s^{-1}.

Since the reaction mechanism of the $D + H_2$ system has been studied in much greater detail compared to that of HD + H we felt that it was probably more appropriate to determine the rate coefficient of the *forward reaction* of equation (46) by applying the principals of detailed balance theory (Watson 1975; Herzberg 1945)

$$r_{HD+H} = r_{H_2+D} \exp\left(\frac{-\Delta E_0}{kT_n}\right) \frac{Q_{tot}(HD)Q_{tot}(H)}{Q_{tot}(D)Q_{tot}(H_2)}, \quad (48)$$

where $Q_{tot} = Q_{trans} Q_{int}$ (i.e., a product of the translational and internal partition function) is the total partition function. The population probabilities for states in HD and H_2 were calculated as described in § 3. $\Delta E_0/k = 418$ K defines the energy difference between the system $HD(v = 0) + H$ and $D + H_2(v = 0)$ at 0 K (Götting et al. 1986).

When gas temperatures of $T_n \gtrsim 2000$ K are reached in the postshock region, molecular hydrogen is dissociated due to collisions with neutrals. We have therefore included the dissociation coefficient for H_2 that is provided by Lepp & Shull (1983). We note that their rates differ significantly from those of Dove et al. (1987) at $n(H_2) = 10^4$ cm^{-3}, whereas they are quite similar at $n(H_2) = 10^6$ cm^{-3} when $T_n = 2000$ K. For heteronuclear molecules such as HD and CO it appears that collision-induced dissociation is a rather slow process (Dalgarno & Roberge 1979; Roberge & Dalgarno 1982; Dalgarno 1985a, b) because these molecules stabilize more efficiently by radiation due to their shorter radiative lifetimes. We have ignored, for the densities considered in this article, that HD can be dissociated by collisions with neutrals because of the small dissociation probability from low-lying vibrational states.

H_2 and HD can also dissociate through ion-neutral collisions when ion and neutral fluids stream through one another at rather high relative drift velocities. We have included this process for both H_2 and HD into our model by adopting equations (41)–(48) of Draine et al. (1983). The polarizability of HD was assumed to be equal to that of H_2. We note that the dissociation rate coefficient for H_2 due to ion-neutral collisions dominated over the rate for neutral-neutral collisions in all our calculations. This effect can be assigned to the fact that at low temperatures $T_n \lesssim 2500$ K dissociations due to neutral-neutral collisions are not very efficient. For HD the situation is different since here the rate coefficient of equation (46) is much faster than that for dissociation due to collision with ions. Furthermore, H_2, HD, H, and to a lesser extent He, can also be ionized through ion-neutral collisions. If the relative drift velocity of the neutral and ion fluid is large enough it may also have an effect on the fractional ionization and subsequently the shock structure. We have therefore also included the formalism of Draine et al. (1983) for the ionization of these species. We note, however, that we did not see any indication of self-ionization effects at high shock speeds ($u_s = 50$ km s^{-1}) and densities ($n_H = 10^4$ cm^{-3}) described by these authors. This may be due to the recombination reactions (see Table 2, below) we included into our model that seem to inhibit any large increases in fractional ionization. In addition to the chemical reactions described above we have included other reactions as summarized in Table 2 (below) that are important for the calculation of the shock structure and HD abundance. For ion-neutral reactions we have introduced an effective temperature (Pineau des Forets et al. 1986) in order to make use of the common notation of published rate coefficients for chemical reactions that are proportional to

$$r \propto \exp\{-\max[\beta/T_{eff}, (\beta - 3T_s)/T_r]\}, \quad (49)$$

where

$$T_{eff} = T_r + T_s, \quad (50)$$

with

$$T_r = \frac{(m_i T_n + m_n T_i)}{(m_i + m_n)} \quad (51)$$

and

$$T_s = \frac{\mu_{in}(u_i - u_n)^2}{3k}. \quad (52)$$

5. MODEL CALCULATIONS

5.1. *Initial Values*

The composition of the preshock gas is given in Table 1, and chemical reactions are given in Table 2. It was assumed that all hydrogen is in molecular form and all deuterium is locked in HD. The latter assumption is based on a very large fractionation effect (Dalgarno 1985; Smith & Adams 1985; Crutcher & Watson 1985) occurring in the cold ISM due to the exoergic nature of the reaction

$$D^+ + H_2 \rightleftharpoons HD + H^+ - \Delta H_0, \quad (53)$$

where $\Delta H_0/k = 464$ K. We neglected that a small fraction of deuterium can also be locked in other molecular species that are mainly synthesized via reactions (Smith, Adams, & Alge 1982)

$$XH^+ + HD \rightleftharpoons XD^+ + H_2, \quad (54)$$

where X is some atomic or molecular constituent. Of equation (54),

$$H_3^+ + HD \rightleftharpoons H_2D^+ + H_2 \quad (55)$$

plays probably the most important role in the cold ISM. The standard value for the CO abundance of $CO/H_2 = 8 \times 10^{-5}$ was adopted. For the abundances of other neutral species we refer to Draine et al. (1983). The ions were assumed to be composed initially of C^+ and I^+ where I^+ has a mass of 28 amu. I^+ represents all ions other than C^+ such as metal ions and possible HCO^+. The abundance of I^+ changed pro-

TABLE 1

PRESHOCK CONDITIONS IN THE INTERSTELLAR MEDIUM

Parameter	Model 1	Model 2	Model 3
$T_n = T_i = T_e$ (K)	30	35	35
B_0 (G)	10^{-4}	3×10^{-4}	10^{-3}
$n(H_2)$ (cm^{-3})	5×10^3	5×10^4	5×10^5
n(HD) (cm^{-3})	1.5×10^{-1}	1.5×10^0	1.5×10^1
n(He) (cm^{-3})	1×10^3	1×10^4	1×10^5
n(CO) (cm^{-3})	4×10^{-1}	4×10^0	4×10^1
n(C) (cm^{-3})	5×10^{-1}	5×10^0	5×10^1
$n(C^+)$ (cm^{-3})	1×10^{-3}	1×10^{-2}	5×10^{-2}
n(O) (cm^{-3})	4.25×10^0	4.25×10^1	4.25×10^2
$n(H_2O)$ (cm^{-3})	0	0	0
n(H) (cm^{-3})	0	0	0
n(D) (cm^{-3})	0	0	0
$n(I^+)$ (cm^{-3})[a]	1×10^{-3}	1×10^{-2}	5×10^{-2}

[a] I^+ was assumed an artificial ion with mass of 28 amu to represent metal ions and/or possible HCO^+.

TABLE 2

CHEMICAL REACTIONS

Reaction	a	b	c	References
$H + CR \rightarrow H^+ + e$	0.46ζ	...	...	1
$H_2 + CR \rightarrow H_2^+ + e$	0.93ζ	...	...	1
$He + CR \rightarrow He^+ + e$	0.50ζ	...	...	1
$H_2 + CR \rightarrow H + H$	0.10ζ	...	...	1
$H_2 + CR \rightarrow H^+ + H + e$	0.022ζ	...	...	1
$D + CR \rightarrow D^+ + e$	0.46ζ	...	...	2
$HD + CR \rightarrow H + D$	0.10ζ	...	...	2
$HD + CR \rightarrow HD^+ + e$	0.93ζ	...	...	2
$C + CR \rightarrow C^+ + e$	1.8ζ	...	...	3
$e + H^+ \rightarrow H$	3.60×10^{-12}	-0.75	...	1
$e + H_2^+ \rightarrow H + H$	8.0×10^{-8}	-0.5	...	1
$e + He^+ \rightarrow He$	4.5×10^{-12}	-0.67	...	4
$e + C^+ \rightarrow C$	1.8×10^{-12}	-0.62	...	1
$e + H_3^+ \rightarrow H_2 + H$	5.0×10^{-9}	-0.5	...	1
$e + H_3^+ \rightarrow H + H + H$	5.0×10^{-9}	-0.5	...	1
$e + CH^+ \rightarrow C + H$	2.9×10^{-7}	-0.4	...	4
$e + H_2D^+ \rightarrow H_2 + D$	3.33×10^{-10}	-0.5	...	2
$e + H_2D^+ \rightarrow HD + H$	3.33×10^{-10}	-0.5	...	2
$e + H_2D^+ \rightarrow D + H + H$	3.33×10^{-10}	-0.5	...	2
$D^+ + H \rightarrow H^+ + D$	1.0×10^{-9}	...	...	2
$H^+ + D \rightarrow D^+ + H$	1.0×10^{-9}	...	4.1×10^{1}	2
$D^+ + H_2 \rightarrow H^+ + HD$	2.1×10^{-9}	...	...	2
$H^+ + HD \rightarrow D^+ + H_2$	1.0×10^{-9}	...	4.64×10^{2}	2
$H_3^+ + D \rightarrow H_2D^+ + H$	1.0×10^{-9}	...	...	2
$H_2D^+ + H \rightarrow H_3^+ + D$	1.0×10^{-9}	...	6.32×10^{2}	2
$H_3^+ + HD \rightarrow H_2D^+ + H_2$	1.7×10^{-9}	...	...	2
$HD^+ + H_2 \rightarrow H_2D^+ + H$	1.05×10^{-9}	...	...	2
$HD^+ + H_2 \rightarrow H_3^+ + D$	1.05×10^{-9}	...	...	2
$H_2D^+ + H_2 \rightarrow H_3^+ + HD$	1.7×10^{-9}	...	1.50×10^{2}	2
$H_2D^+ + C \rightarrow CH^+ + HD$	1.0×10^{-9}	...	...	2
$H^+ + He \rightarrow He^+ + H^+ + e$	8.63×10^{-14}	0.43	2.85×10^{5}	1
$H^+ + C \rightarrow C^+ + H^+ + e$	5.9×10^{-13}	0.4	1.31×10^{5}	1
$H^+ + CH \rightarrow CH^+ + H^+ + e$	8.83×10^{-14}	0.5	1.29×10^{5}	1
$H^+ + H_2 \rightarrow H_2^+ + H$	6.4×10^{-10}	...	2.13×10^{4}	1
$H_2^+ + H \rightarrow H^+ + H_2$	1.0×10^{-10}	...	...	1
$H^+ + CH \rightarrow CH^+ + H$	1.9×10^{-9}	...	...	1
$He^+ + HD \rightarrow H^+ + D + He$	5.5×10^{-14}	-0.24	...	2
$He^+ + HD \rightarrow D^+ + H + He$	5.5×10^{-14}	-0.24	...	2
$He^+ + H \rightarrow H^+ + He$	1.9×10^{-15}	...	...	1
$He^+ + H_2 \rightarrow H^+ + H + He$	1.1×10^{-13}	...	...	1
$He^+ + H_2O \rightarrow H^+ + OH + He$	2.03×10^{-10}	...	...	1
$He^+ + CO \rightarrow C^+ + O + He$	1.7×10^{-9}	...	...	1
$He^+ + OH \rightarrow O^+ + H + He$	1.1×10^{-9}	...	...	4
$He^+ + O_2 \rightarrow O^+ + O + He$	1.1×10^{-9}	...	...	1
$He^+ + CH \rightarrow C^+ + H + He$	1.1×10^{-9}	...	...	4
$C^+ + H_2 \rightarrow CH^+ + H$	2.0×10^{-10}	...	4.64×10^{3}	1
$H_2^+ + H_2 \rightarrow H_3^+ + H$	2.1×10^{-9}	...	...	1
$H_2^+ + H_2 \rightarrow H^+ + H_2 + H$	4.17×10^{-11}	0.5	3.07×10^{4}	1
$H_2^+ + C \rightarrow CH^+ + H$	2.4×10^{-9}	...	...	4
$H_2^+ + CH \rightarrow CH^+ + H_2$	7.1×10^{-10}	...	...	4
$H_3^+ + H \rightarrow H_2^+ + H_2$	2.08×10^{-9}	...	1.88×10^{4}	1
$H_3^+ + H_2 \rightarrow H_2^+ + H_2 + H$	3.41×10^{-11}	0.5	7.16×10^{4}	1
$H_3^+ + H_2 \rightarrow H^+ + H_2 + H_2$	3.41×10^{-11}	0.5	5.04×10^{4}	1
$H_3^+ + C \rightarrow CH^+ + H_2$	2.0×10^{-9}	...	...	4
$CH^+ + H \rightarrow C^+ + H_2$	6.0×10^{-10}	-0.25	...	1
$H + H \rightarrow H_2$	8.14×10^{-17}	0.5	...	2
$H + D \rightarrow HD$	5.72×10^{-17}	0.5	...	2
$C + H_2 \rightarrow CH + H$	4.5×10^{-11}	0.5	1.56×10^{4}	1
$C + OH \rightarrow CO + H$	1.11×10^{-10}	0.5	...	1
$C + H_2O \rightarrow CH + OH$	1.43×10^{-10}	0.5	2.4×10^{4}	1
$C + O_2 \rightarrow CO + O$	1.8×10^{-11}	0.5	...	1
$O + CH \rightarrow CO + H$	9.53×10^{-11}	0.5	...	1
$O + CH \rightarrow C + OH$	1.73×10^{-11}	0.5	4×10^{3}	1
$O + OH \rightarrow O_2 + H$	4.33×10^{-11}	-0.5	3×10^{1}	1
$O + H_2O \rightarrow OH + OH$	1.35×10^{-12}	1.75	7.86×10^{3}	1
$O + CO \rightarrow C + O_2$	2.9×10^{-11}	0.5	6.93×10^{4}	1
$O + H_2 \rightarrow OH + H$	1.5×10^{-13}	2.8	2.98×10^{3}	4
$CH + H \rightarrow C + H_2$	1.8×10^{-11}	0.5	4×10^{3}	1
$CH + OH \rightarrow H_2O + C$	1.0×10^{-10}	...	...	1
$OH + H \rightarrow O + H_2$	6.6×10^{-13}	1.53	2.97×10^{3}	1

TABLE 2—*Continued*

Reaction	*a*	*b*	*c*	References
$OH + H_2 \rightarrow H_2O + H$	8.8×10^{-13}	1.95	1.42×10^3	1
$OH + OH \rightarrow H_2O + O$	4.2×10^{-12}	...	2.42×10^2	1
$H_2O + H \rightarrow OH + H_2$	7.44×10^{-12}	1.57	9.14×10^3	1
$CO + H \rightarrow OH + C$	1.11×10^{-10}	0.5	7.77×10^4	1
$CO + H \rightarrow CH + O$	9.53×10^{-11}	0.5	8.83×10^4	1
$O_2 + H \rightarrow OH + O$	1.63×10^{-9}	−0.9	8.75×10^3	1
$H + H_2 \rightarrow H + H + H$[a]				
$H_2 + H_2 \rightarrow H_2 + H + H$[a]				
$H + HD \rightarrow H_2 + D$[b]				
$D + H_2 \rightarrow HD + H$[b]				

NOTES.—The reaction rates are in the form $a(T/300\text{K})^b \exp(c/T)$ cm^3s^{-1}. For the evaluation of T see text. In case of cosmic-ray (CR) reactions the rates are in the form $a\zeta$ s^{-1} where ζ is the primary cosmic-ray ionization rate. A blank for b and c denotes a zero.

[a] See text.

[b] See eq. (46).

REFERENCES.—(1) Hollenbach & McKee 1989; (2) Pineau des Forets et al. 1989; (3) de Jong et al. 1980; (4) Pineau des Forets et al. 1986.

portionally to u_s/u_i over the shock region. The values for the strength of the magnetic field was adopted from Draine et al. (1983).

5.2. *Computational Methods*

Since in C shocks all variables are continuous their computation can be executed as an initial value problem. The program was started from equilibrium values upstream ($u_n = u_s$) with the exception that $u_i = (1 - \delta)u_s$ with $\delta < 2 \times 10^{-4}$. The results of the model calculations were insensitive to this perturbation. Moreover, the assumed kinetic temperatures (see Table 1) for the cold ISM did not have an effect on the calculated line strengths. The coupled, first-order, nonlinear ordinary equations as of § 2.1 were solved with a variable-order variable-step Gear differential equation solver provided by the NAG FORTRAN library. The postshock region was divided in a nonuniform mesh in which the cooling functions, the level population probabilities, and the chemistry including the fractional ionization was calculated at each grid point. The density of the mesh was chosen such that errors in line intensities remained smaller than a few percent when the mesh density was even further increased. The line intensities of H_2 and HD were calculated by integration along z. We have investigated three cases of preshock conditions (see Table 1) for densities of $n_H = 10^4$, 10^5, and 10^6 cm^{-3} and shock speeds from 15 to 45 km s^{-1}.

5.3. *Uncertainties*

We now address the simplifications and uncertainties of some of the variables we employed in our calculations. In § 3 we have included the rate coefficients for the vibrational deexcitation of HD by collision with H_2, He, and H by introducing $\alpha = 2$. We notice that the relaxation times in M–HD and M–H_2 (Simpson et al. 1975) were measured at only two temperatures. It is, therefore, possible that the value of α might deviate from 2 at temperatures other than $1600 < T_n < 2000$ K. However, we point out that most of the line emission in the $v = 1 \rightarrow 0$ band emanates from a postshock region, where the value of T_n is in that order. Actually, T_n hardly exceeded 2500 K in all our computations. We were interested in testing the actual sensitivity of the line intensities in the HD $v = 1 \rightarrow 0$ band upon changes of that deexcitation rate coefficient. Therefore, we run additional computations where $\alpha = 1$. We notice that for the highest shock speeds $u_s \gtrsim 40$ km s^{-1} and densities $n_H \approx 10^6$ cm^{-3} the line intensities decreased by about 25%, whereas for smaller shock speeds and densities the change in the deexcitation rate also translated into a decrease in line emission by a factor of 2. This effect can be assigned to much faster radiative transition rates compared to those for collisional deexcitation at low shock speeds and densities. This implies that except at the highest shock velocities and densities that were considered vibrational levels in HD are subthermally populated. It also means that at low shock velocities and densities collisional deexcitation rates have to be more reliable and additional data on the vibrational deexcitation rates of HD are urgently needed. However, at low shock speeds rotational transitions appear to be much more intense than vibrational transitions.

Although it was not the intention of this paper to calculate the line emission of H_2, we should point out that the assumed ortho/para-H_2 ratio of 3 is an assumption that may not always apply at low densities and temperatures. In a true equilibrium case, however, one should model a level-dependent formation entry rate that commences with the initial condition where, depending on the preshock density, most of the H_2 is found in the lowest (para) level. It would, therefore, be of great interest how fast the assumed ortho/para ratio is reached when the gas is heated. To our knowledge this has never been demonstrated. Instead we may quote the result of Dalgarno, Black, & Weisheit (1973) who show that ortho- and para-hydrogen can mix efficiently by rapid proton interchange collisions in dense interstellar clouds. H^+ and H_3^+ is produced in the ISM by cosmic rays. The atom-atom interchange reaction $H + H_2(J = 0) \rightarrow H_2(J = 1) + H$ (Mandy & Martin 1991), however, is much slower due to a higher energy threshold. A measurement of H + para-$H_2 \rightarrow$ ortho-H_2 + H by Schofield (1967) implies a reaction rate of $8.0 \times 10^{-11} \exp(-3889\ \text{K}/T_n)$ cm^3 s^{-1}. A very rough estimate for the time in which an equilibrium can be reached is about $t_{\text{equilib}} \sim 10^8$ s ($z \approx 4 \times 10^{14}$ cm at $u_s = 40$ km s^{-1}) for $n = 10^4$ cm^{-3} and $T_n = 1000$ K. In any event, for densities considered in the present model a value of 3 for the ortho/para ratio should not be far from reality once the gas starts to heats up.

For other uncertainties such as in the fractional ionization in the ISM we refer to a more general treatment in the literature. We should point out that the strength of the magnetic field in

the preshock gas (i.e., in star-forming regions) may be lower than the values assumed in the present paper. We performed additional model calculations with reduced magnetic field strengths, which were just above critical values (Draine et al. 1983). Our results showed that the postshock regions were compressed, whereas the peak temperature of the gas achieved higher values. The reduced extension of the postshock gas implied also smaller H_2 and HD line intensities. In some instances, however, higher line intensities for vibrational transitions were observed. This effect was seen when the high gas temperature could offset the reduced extension of the postshock region. In some star-forming regions the magnetic field strengths may also be smaller than the critical value required to maintain C type shocks. We have not treated this case in the present paper since this requires J type shocks with magnetic precursors.

6. RESULTS

Figures 1*a* and 1*b* depict the structure across the postshock regions for initial conditions as of model 1 and 3, respectively, where the shock speed is $u_s = 40$ km s^{-1}. It is seen that with rapidly increasing n(H), which originates from the dissociation of H_2, a fraction of the HD is destroyed. However, once enough deuterium is produced, which itself reacts with H_2, an equilibrium between the production and destruction of HD is maintained. As the postshocked gas cools down this equilibrium shifts toward the left side of equation (46) implying that some of the deuterium can be converted again to HD. The consequence of this temporal conversion to deuterium is that the intensity of HD line emission is somewhat lower in the shocked gas as one would have inferred from the initial HD abundance. For lines in the HD $v = 1 \rightarrow 0$ band that emanate mainly from hot gas with $T_n > 1000$ K this effect is greater than for transitions in the $v = 0 \rightarrow 0$ band that originate mainly from cooler regions of the gas where the HD can reform again. The same effect basically applies also to H_2. The only difference being, however, that H_2 cannot be synthesized as fast as HD. For low shock speeds the situation is different because due to the low relative velocity of the neutral and ion fluids less molecular hydrogen is dissociated that thus can participate in the destruction of HD. About 73%, 63%, and 62% of all deuterium is still found in the form of HD after a shock front with $u_s = 40$ km s^{-1} has traveled through the ISM when the preshock densities are as of model 1, 2, and 3, respectively. For a shock wave with $u_s = 25$ km s^{-1}, less than 1% of the HD is converted to D for all three model cases.

Figures 2 and 3 display the intensities of selected H_2 and HD emission lines versus shock speed for three different preshock densities. We considered the $v = 1 \rightarrow 0$ $P(2)$, $P(3)$, $P(4)$, $R(1)$, $R(3)$, $R(4)$ lines of HD and the $S(1)$ line of H_2 and for the $v = 0 \rightarrow 0$ bands the $R(4)$, $R(5)$, $R(8)$, and $R(9)$ lines of HD and the $S(2)$ and $S(3)$ lines of H_2. The wavelengths of the HD $v = 1 \rightarrow 0$ transitions $R(1)$, $R(3)$, $R(4)$, $P(2)$, $P(3)$, and $P(4)$ are 2.632, 2.535, 2.494, 2.898, 2.980, and 3.069 μm, respectively. For the pure rotational transitions $R(4)$, $R(5)$, $R(8)$, and $R(9)$ the rest wavelengths are 23.0338, 19.4305, 13.5927, and 12.4718 μm (Ulivi, De Natale, & Inguscio 1991). These lines were chosen because they can be observed in principle, with more or less interference by telluric absorption lines, even from ground-based telescopes or from above the Earth's troposphere (see also Figs. 4 and 5). The results for radiative transitions in HD other than those presented here can be requested from the author. In addition to the calculation of the absolute intensities of HD line emission we tested whether its preshock abundance can be deduced from the strength of the emission lines. Therefore, we have run further computations with abundances of $10^{-5} < \mathrm{HD}/\mathrm{H}_2 < 8 \times 10^{-5}$. It turned out that within this range the line intensities can be directly scaled to the preshock abundance of HD, thus allowing a determination of the HD abundance from its line strengths. However, it seems necessary to derive or constrain shock parameters such as the total density and shock speed from other tracers.

Of all radiative transitions in the HD $v = 1 \rightarrow 0$ band those of the R branch were found to be the strongest except for preshock densities $n(\mathrm{H}) < 10^5$ cm^{-3}. As one would have expected from the nature of the molecules HD and H_2 the transition intensities of HD behave very similarly to that of H_2 lines. However, slight differences occur due to different chemistries and collisional excitation rates. It should be noted that the energies for the HD $J = 9$ and 10 levels are roughly comparable to the energy difference between the first vibrational and the ground state of HD. It implies that the $R(8)$ and $R(9)$ line

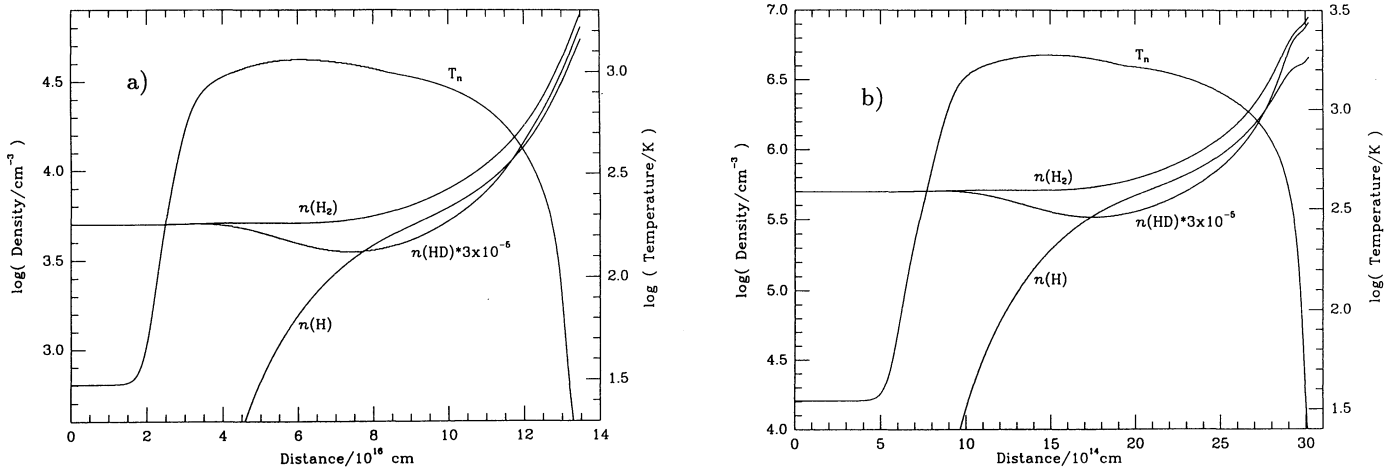

FIG. 1.—(*a*) Kinetic temperature (T_n), number densities of atomic n(H), molecular hydrogen $n(H_2)$, and deuterated hydrogen n(HD) as a function of distance behind the shock front. The shock speed was $u_s = 40$ km s^{-1} and preshock conditions as of model 1 (see Table 1). (*b*) Same as (*a*), but for model 3.

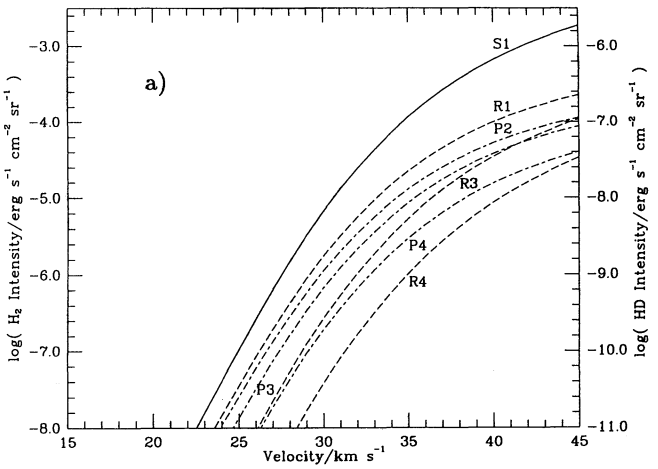

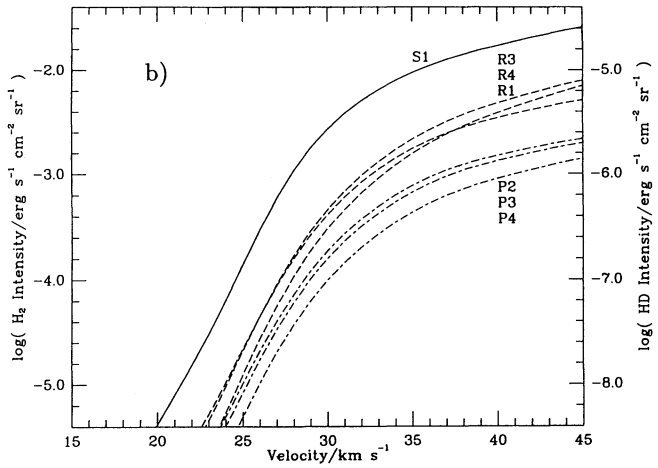

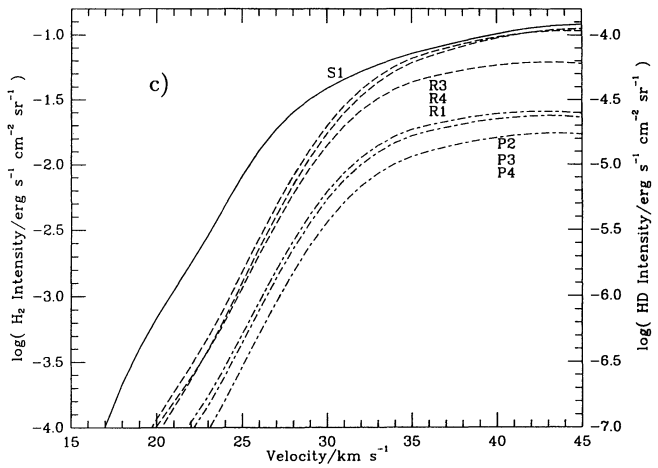

FIG. 2.—(*a*) Intensities of the $v = 1 \rightarrow 0$ $S(1)$ transition of H_2 (*solid line*) and $R(1)$, $R(3)$, $R(4)$ (*dashed lines*), and $P(2)$, $P(3)$, $P(4)$ (*short-long dashed lines*) transitions of HD vs. shock velocity. Preshock conditions are as of model 1. Note the different scales for the *y*-axes. (*b*) Same as (*a*), but for model 2. (*c*) Same as (*a*), but for model 3.

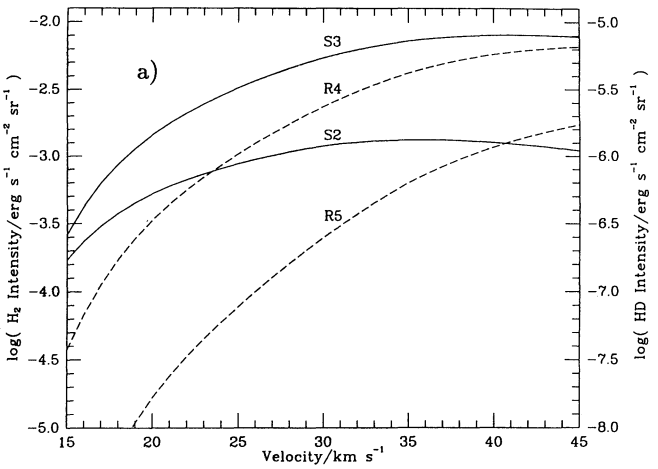

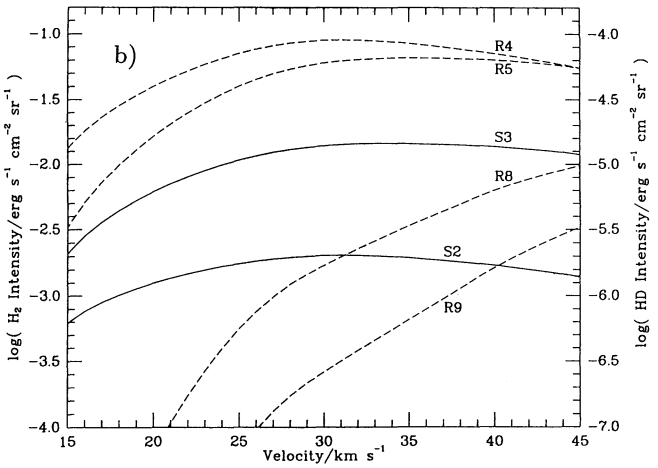

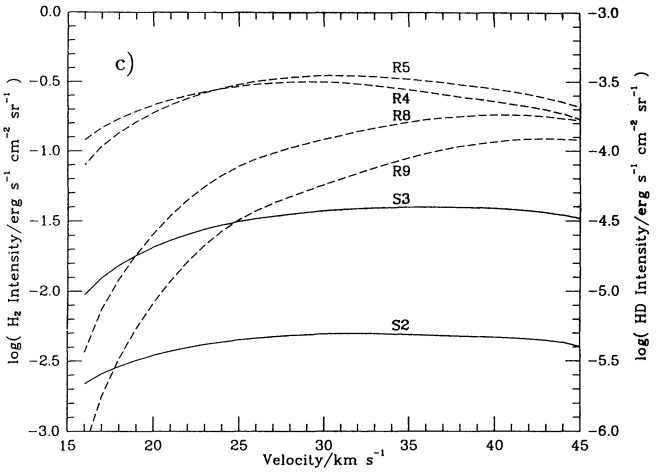

FIG. 3.—(*a*) Intensities of the $v = 0 \rightarrow 0$ $S(2)$ and $S(3)$ transitions of H_2 (*solid lines*) and $R(4)$, $R(5)$, $R(8)$, $R(9)$ transitions of HD (*dashed lines*) as a function of shock velocity. Preshock conditions are as of model 1. (*b*) Same as (*a*), but for model 2. (*c*) Same as (*a*), but for model 3.

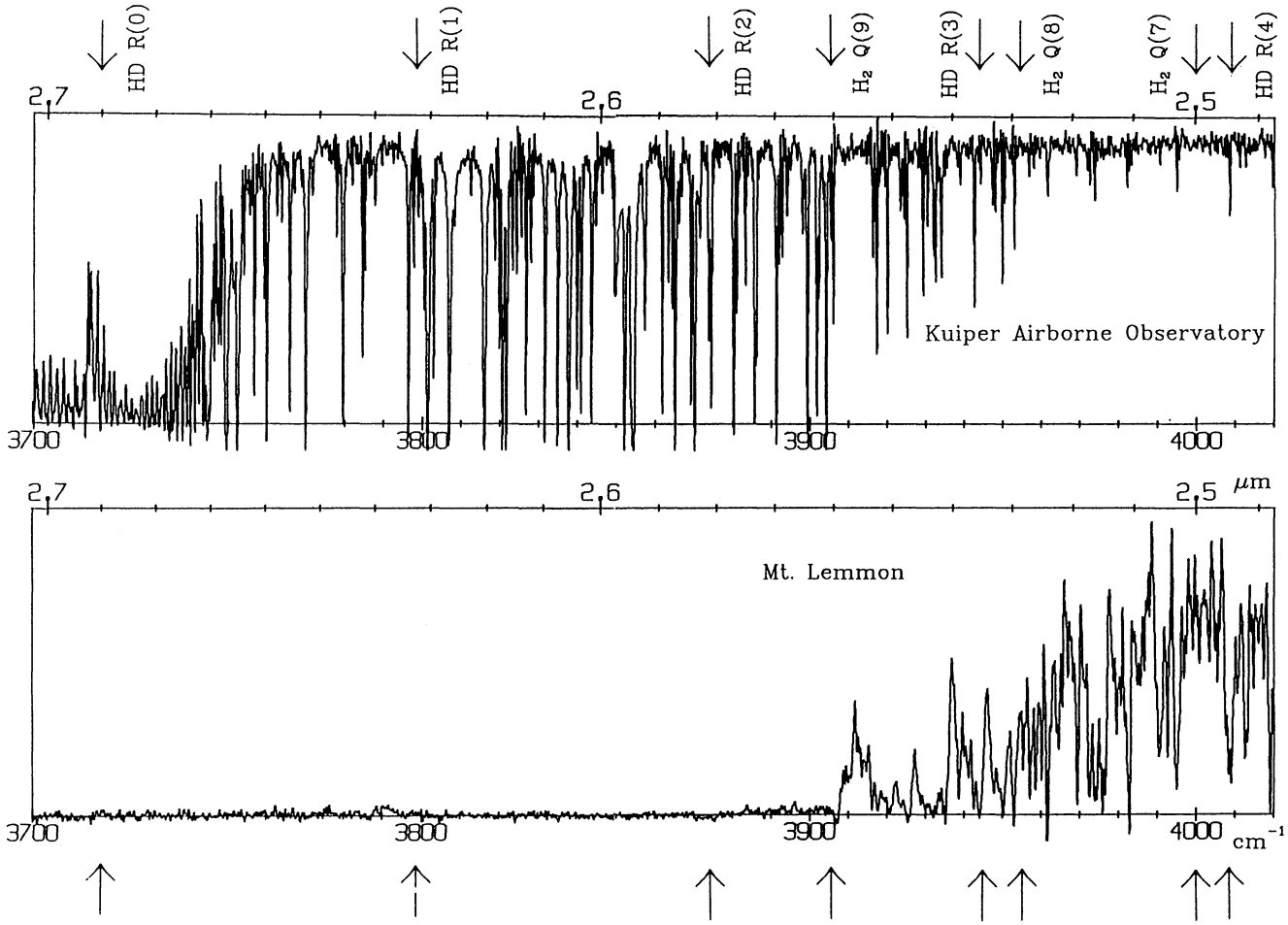

FIG. 4.—Atmospheric transmission spectra (R = 14,300) from 2.5 to 2.7 μm recorded with the Arizona high-resolution FTS (Davis et al. 1980) at Mount Lemmon and from aboard the KAO. The spectra are not corrected for instrumental transmission. The transitions in the first fundamental of HD and H_2 are indicated by arrows.

intensities tend to react very sensitively to changes in preshock densities, whereas transitions from lower lying levels are not so much affected. The $R(8)$ and $R(9)$ lines, if detectable, might thus serve also as density tracers.

7. DISCUSSION

We now address the question whether IR line emission of HD from shocked molecular gas is observable with currently available IR spectrometers. It appears that the observation of emission lines in the $v = 1 \rightarrow 0$ band is more or less hampered by the interference of telluric absorption lines. In Figure 4 we display atmospheric transmission spectra in the wavelength region from 2.5 to 2.7 μm recorded at the 60 inch telescope on Mount Lemmon and the 36 inch telescope aboard the Kuiper Airborne Observatory (KAO) at altitudes of 2800 and 12,500 m, respectively (Larson 1991). The observed object was the moon. The amount of precipitable water above these sites is usually of the order 0.01 and 5 mm for the KAO and Mount Lemmon, respectively. It can be seen that the $R(0)$, $R(1)$, and $R(2)$ lines cannot be observed from ground-based telescopes, whereas the $R(1)$ line exhibits little interference when observed from above the troposphere. The $R(3)$ and $R(4)$ lines could be observed in principle with ground-based telescopes. However, it depends on the amount of precipitable water and the object's radial velocity whether an appreciable atmospheric transmission can be achieved. Dry atmospheric conditions are also a necessary requirement for observations of the rotational lines. For the transmittances at these wavelengths we utilized an atmospheric modeling program (Lord 1992) where we assumed an altitude of 4.2 km, a water column density of 1 mm precipitable water and an air mass of $z = 1.41$ (see Fig. 5).

Assuming an atmospheric transmittance of unity we define a detection limit (3 σ) for an emission line in the first vibrational band of HD from an extended source to

$$I = 6.5 \times 10^{-6} \left(\frac{t}{1\ \mathrm{hr}}\right)^{-1/2} \left(\frac{D}{3\ \mathrm{m}}\right)^{-2} \mathrm{ergs\ s^{-1}\ cm^{-2}\ sr^{-1}}\ , \quad (56)$$

where t is the total integration time and D is the diameter of the telescope. The spectral resolution was assumed to be R = 5000 and FOV = 4″(field of view). It turns out that basically all considered transitions should be observable within 1 hour of integration time for $u_s > 30$ km s^{-1} and preshock conditions as of model 3, whereas for a 10 times lower preshock density (model 2) only the $R(3)$ and $R(4)$ lines may be detectable when $u_s > 40$ km s^{-1}. No HD emission lines may be detected for model 1.

In order to evaluate the required integration time to detect rotational transitions in the HD $v = 0 \rightarrow 0$ band the forefactor

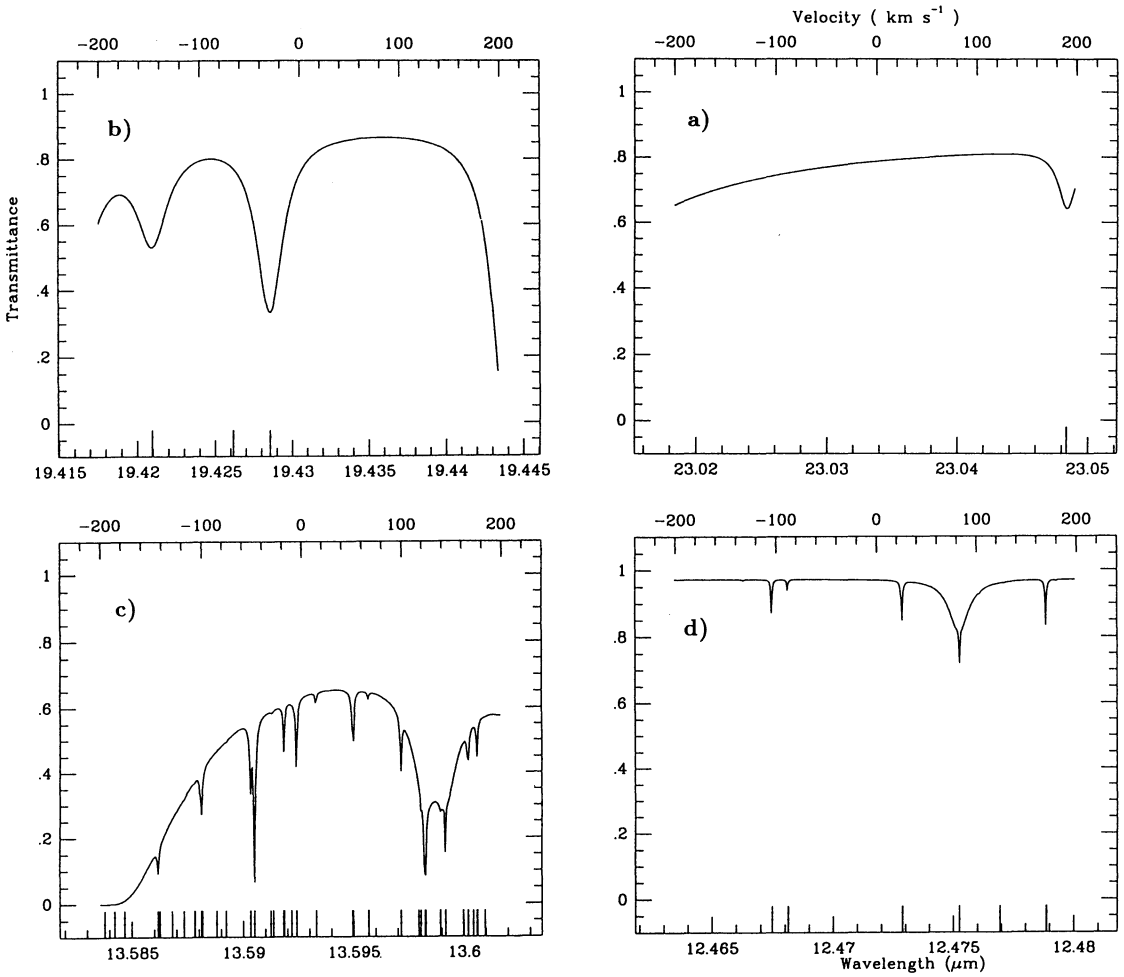

FIG. 5.—Model atmospheric transmittance spectra for rotational lines (*a*) *R*(4), (*b*) *R*(5), (*c*) *R*(8), and (*d*) *R*(9) of HD ± 200 km s^{-1} of the line center. The bars at the *x*-axis indicate absorption lines due to H_2O, O_2, and O_3. For model parameters see text.

of equation (56) becomes $\sim 8 \times 10^{-5}$ for $\lambda = 15$ μm and FOV = 10″. For model 3 the *R*(4) and *R*(5) transitions may be observable also at the lowest considered shock velocities, whereas the *R*(8) and *R*(9) line become only detectable for $u_s \gtrsim 30$ km s^{-1}. For model 2 the *R*(4) and *R*(5) lines may be barely detectable. Similarly, rotational lines of HD cannot be probed when the density in the ISM is as in model 1. All these limits change with HD abundances different than that considered here.

For *ISO* the situation appears to be much better due to the absence of background-induced noise, particularly in the mid-IR. We estimated the detection limit (5 σ) for the short wavelength (SWS) grating and Fabry-Perot spectrometer to about $(1\text{–}5) \times 10^{-7}$ and $(2.5\text{–}1.3) \times 10^{-4}$ ergs s^{-1} cm^{-2} sr^{-1} for the 23 to 12 μm wavelength range, respectively, where 1 hr of pure integration time in a 20″ beam was assumed at *no* continuum radiation. Radiative transitions in the first fundamental band of HD were not considered for *ISO* because the resolution of the grating spectrometer might be just too low ($R < 2000$) to unambiguously identify the faint HD lines. If we assume an astronomical source with low continuum emission, which certainly does not always apply, *ISO* would allow also the detection of the *R*(4) and *R*(5) lines from shocked molecular gas that is less dense (model 1). *ISO* offers the unique opportunity to observe radiative transitions of HD that are not observable from ground-based telescopes. This occasion ought to be used to shed light on an important species such as deuterium.

We would like to thank John Black, Harold Larson, and Frank Bertoldi for their critical comments and suggestions. This research was supported in part by the NASA grant NAG2-206.

REFERENCES

Abgrall, H., Roueff, E., & Viala, Y. 1982, A&AS, 50, 505
Bragg, S. L., Brault, J. W., & Smith, W. H. 1982, ApJ, 263, 999
Continetti, R. E., Balko, B. A., & Lee, Y. T. 1990, J. Chem. Phys., 93, 5719
Crutcher, R. M., & Watson, W. D. 1985, in Molecular Astrophysics, ed. G. H. F. Diercksen, W. F. Huebner, & P. W. Langhoff (NATO ASI Series C, Vol. 157), 255
Dalgarno, A. 1985a, in Molecular Astrophysics, ed. G. H. F. Diercksen, W. F. Huebner, & P. W. Langhoff (NATO ASI Series C, Vol. 157), 3
———. 1985b, in Molecular Astrophysics, ed. G. H. F. Diercksen, W. F. Huebner, & P. W. Langhoff (NATO ASI Series C, Vol. 157), 281
Dalgarno, A., Black, J. H., & Weisheit, J. C. 1973, Astrophys. Lett., 14, 77
Dalgarno, A. & Roberge, W. G. 1979, ApJ, 233, L25

Danby, G., Flower, D. R., & Monteiro, T. S. 1987, MNRAS, 226, 739
Davis, D. S., Larson, H. P., Williams, M., Michel, G., & Connes, P. 1980, Appl. Opt., 19, 4138
de Jong, T., Dalgarno, A., & Boland, W. 1980, A&A, 91, 68
Draine, B. T 1980, ApJ, 241, 1021
———. 1987, Princeton Observatory Preprints, POB-213
Draine, B. T., Roberge, W. G., & Dalgarno, A. 1983, ApJ, 264, 485
Dove, J. E., Rusk, A. C. M., Cribb, P. H., & Martin, P. G. 1987, ApJ, 318, 379
Elitzur, M., & Watson, W. D. 1978, A&A, 70, 443
Flower, D. R., Pineau des Forets, G., & Hartquist, T. W. 1985, MNRAS, 216, 775
———. 1986, MNRAS, 218, 729
Götting, R., Mayne, H. R., & Toennies, J. P. 1986, J. Chem. Phys., 85, 6396
Herzberg, G. 1945, Molecular Spectra And Molecular Structure. II. Infrared and Raman Spectra of Polyatomic Molecules (Princeton: Van Nostrand)
Hollenbach, D., & McKee, C. F. 1979 ApJS, 41, 555
———. 1989 ApJ, 342, 306
Larson, H. P. 1991, private communication
Laurent, C., Vidal-Madjar, A., & York, D. G. 1979, ApJ, 229, 923
Lepp, S., & Shull, J. M. 1983, ApJ, 270, 578
Linsky, J. L., et al. 1993, ApJ, 402, 694
Linsky, J. L., Diplas, A., Ayres, T. R., Wood, B., & Brown, A. 1994, BAAS, 25, 1464
Lord, S. D. 1992, NASA Tech. Mem. 103957
Mandy, M. E., & Martin, P. G. 1991, J. Phys. Chem., 95, 8726
Margolis, J. S. 1980, in Vibrational-Rotational Spectroscopy for Planetary Atmospheres, ed. M. J. Mumma, K. Fox, & J. Hornstein (NASA CP 2233, Vol. II), 431
McCollough, R. P. 1992, ApJ, 390, 213
McKee, C. F., Storey, J. W. V., Watson, D. M., & Green, S. 1982, ApJ, 259, 647
McKellar, A. R. W., Goetz, W., & Ramsey, D. A. 1976, ApJ, 207, 663
Mitchell, D. E., & LeRoy, S. 1973, J. Chem. Phys., 58, 3449
Neufeld, D. A., & Melnick, G. J. 1987, ApJ, 322, 266
Osterbrock, D. E. 1961, ApJ, 134, 270
Pineau des Forets, G., Flower, D. R., Hartquist, T. W., & Dalgarno, A. 1986, MNRAS, 220, 801
Pineau des Forets, G., Roueff, E., & Flower, D. R. 1989, MNRAS, 240, 167
Rabitz, H., & Zarur, G. 1975, J. Chem. Phys., 62, 1425
Roberge, W., & Dalgarno, A. 1982, ApJ, 255, 176
Rozenshtein, V. B., Gershenzon, Yu. M., Ivanov, A. V., Il'in, S. D., Kucheryavii, S. I., & Umanskii, S. Ya. 1985, Chem. Phys. Lett., 121, 89
Schaefer, J. 1990, A&AS, 85, 1101
Schofield, K. 1967, Planet. Space Sci., 15, 643
Shavitt, I. 1959, J. Chem. Phys., 31, 1359
Shull, J. M., & Beckwith, S. 1982, ARA&A, 20, 163
Simpson, C. J. S. M., Price, T. J., & Crowther, M. E. 1975, Chem. Phys. Lett., 34, 181
Sternberg, A. 1990, ApJ, 361, 121
Smith, D., & Adams, N. G. 1985, in Molecular Astrophysics, ed. G. H. F. Diercksen, W. F. Huebner, & P. W. Langhoff (NATO ASI Series C, Vol. 157), 453
Smith, D., Adams, N. G., & Alge, E. 1982, ApJ, 263, 123
Smith, M. D., & Brand, P. W. J. L. 1990a, MNRAS, 242, 495
———. 1990b, MNRAS, 243, 498
Tarr, S. M., & Rabitz, H. 1979, J. Chem. Phys., 70, 2569
Turner, J., Kirkby-Docken, K., & Dalgarno, A. 1977, ApJS, 35, 281
Ulivi, L., De Natale, P., & Inguscio, M. 1991, ApJ, 378, L29
Vidal-Madjar, A., Ferlet, R., Laurent, C., & York, D. G. 1982, ApJ, 260, 128
Vidal-Madjar, A., Laurent, C., Bonnet, R. M., & York, D. G. 1977 ApJ, 211, 91
Vidal-Madjar, A., Laurent, C., Gry, C., Bruston, P., Ferlet, R., & York, D. G. 1983, A&A, 120, 58
Watson, W. D. 1975, in Atomic and Molecular Physics And The Interstellar Matter, ed. R. Balian, P. Encrenaz, & J. Lequeux (Les Houches, Session 26) (Elsevier: North-Holland), 181
Westenberg, A. A., & de Haas, N. 1967, J. Chem. Phys., 47, 1393
Wright, E. L., & Morton, D. C. 1979, ApJ, 227, 483
York, D. G., & Rogerson, J. B. 1976, ApJ, 203, 378
Zhang, J. Z. H., & Miller, W. H. 1989, J. Chem. Phys., 91, 1528